Template Synthesis of Nanowires in Porous Polycarbonate Membranes: Electrochemistry and Morphology

C. Schönenberger,*,†,‡ B. M. I. van der Zande,† L. G. J. Fokkink,† M. Henny,‡ C. Schmid,‡ M. Krüger,‡ A. Bachtold,‡ R. Huber,‡ H. Birk,†,‡ and U. Staufer‡

Philips Research Laboratories, Professor Holstlaan 4, NL-5656 AA Eindhoven, The Netherlands, and University of Basel, Department of Physics and Astronomy, Klingelbergstrasse 82, CH-4056 Basel, Switzerland

Received: November 27, 1996; In Final Form: March 24, 1997[⊗]

The potentiostatic electrochemical template synthesis of nanowires (Ni, Co, Cu, Au, and polyporrole) in polycarbonate track-etched membranes with nominal pore diameters d_N between 10 and 200 nm is studied. Along the wire the cross section is found to vary: the wire diameter, which is argued to directly reflect the pore diameter, is observed (for all deposits) to be substantially larger in the middle than at both ends. Therefore, the pores are not cylindrical with constant cross-section, in general, but appear to be "cigarlike". Inside the membrane, the pores are wider by up to a factor 3. Comparing the potentiostatically measured current-time characteristics obtained during wire growth for different pore dimensions, a pore-size dependence of the diffusion coefficient D for the metal ions is found: $D = 2.5, 1.5,$ and 0.7×10^{-6} cm^2/s for $d_N = 80, 30,$ and 10 nm, respectively.

1. Introduction

Template synthesis is an elegant chemical approach for the fabrication of nanostructures, in particular for different kinds of nanowires.[1] It can be considered an alternative to conventional lithography methods. Arrays of nanowires are obtained by filling a porous template that contains a large number of straight cylindrical holes with a narrow size distribution. Filling proceeds in solution by electrochemical deposition[1−4] or other chemical methods,[1] e.g., polymerization reactions, or by high-pressure injection of a melted material.[5] Useful templates are alumite membranes (anodized aluminum films)[6] or track-etched membranes[7] and nanochannel array glass[8] or mesoporous channel hosts.[9] The first two are commercially available.[10]

Historically, the method was introduced by Possin who prepared different metallic wires with diameters as small as 40 nm in pores of etched nuclear damage tracks in mica.[2] The method was thereafter refined by Williams and Giordano who obtained Ag wires with diameters below 10 nm.[3] Membranes filled with Co, Ni, or Fe are magnetic nanocomposites that have a strong perpendicular magnetic anisotropy suitable for perpendicular recording.[11] Penner and Martin demonstrated the successful synthesis of conducting polymers (pyrrole and polythiophene) from commercial screen membranes, which are polycarbonate foils with pores obtained by etching nuclear damage tracks.[4,12] For small pore diameters, the conductivity of these polymeric fibrils was found to be almost an order of magnitude higher than in bulk polymers prepared by the same method. This has been attributed to polymer chains with an enhanced order having less defects due to the unidirectional growth imposed by the confined geometry. Instead of wires, it is also possible to synthesize tubules.[1b] In addition, pores have successfully been filled with two different materials which were stacked alternatingly to form multilayers.[13]

Applications of template synthesis include arrays of electron field emitters, biosensors,[14] novel magnetic-disk materials,[11] magnetic sensors based on the giant magneto-resistance effect,[13]

anisotropic optical filters,[15] and the synthesis of aqueous dispersions of monodisperse metallic colloidal rods.[16]

In this work, the electrochemical growth of nanowires obtained from commercially available polycarbonate track-etched membranes is studied. These membranes are used in many laboratories as filters and are therefore widely available. In recent publications the pores have been assumed to be cylindrical with an inner diameter that corresponds to the one tabulated by the manufacturer (nominal diameter). This hypothesis was only challenged by Chlebny et al.[17] who found that the diameters of nanowires analyzed by transmission electron microscopy (TEM) could be larger by up to a factor of 3 compared to the nominal diameter of the nanopores. In the present paper, the shape of different metallic wires is studied and compared with the electrochemical current during potentiostatic growth. We find (a) in general wires that are *not* cylindrical, (b) a current versus growing time characteristic, and (c) ionic diffusion, which depend on the nominal pore diameter. It is emphasized that the true wire cross-section is an important calibration parameter in all previous studies. For example, it determines the estimated conductivity of conducting polymers grown in pores.[12]

2. Experimental Section

PVP coated polycarbonate screen membranes (overall diameter 13 mm) are used with pore diameters $d_N = 10, 30, 50, 80$ and 200 nm specified by the manufacturer, thereafter refered to as the "nominal diameter" d_N. Results shown in this work have been obtained for membranes from Poretics.[10] Similar results have also been measured for membranes from other suppliers, i.e., Nuclepore and Millipore, confirming that our findings are general. The membranes have a thickness of $L = 6\ \mu$m. A metallic layer serving as back electrode is electron-beam evaporated onto one side of the membrane: a 20-nm adhesion layer of either Ti or Cr is applied first, followed by a Au film with a thickness of 500 nm to 1 μm. The thicker layer is needed in case of the wider pores in order to ensure that the electrode completely covers the pores. After evaporation, the membranes are fixed with the electrode facing down onto a conducting substrate (Cu or Au covered plate) using an adhesive

* Address correspondence to this author at the University of Basel.
† Philips Research Laboratories.
‡ University of Basel.
⊗ Abstract published in *Advance ACS Abstracts,* June 1, 1997.

sticker. This sticker leaves the central part of the membrane open over a diameter of 6 mm, which is the part that is exposed to the electrolyte.

Before mounting the prefixed membrane into the electrochemical cell, it is immersed in deionized water under ultrasonic agitation during 2 min. This step has turned out to be crucial for obtaining reproducible results and a homogeneous growth over the whole 6-mm growing area. If this step is omitted, growth starts in some pores first and the number of pores in which growth proceeds may increase with time, which results in an increasing current (potentiostatic mode). This current increase is an artifact and cannot be related to the effective pore diameter, since at no time is one certain about the number of pores in which electroplating commences. After the ultrasonic treatment, the membranes are withdrawn from the deionized water. A reliable test of successful pore wetting is the requirement that the free membrane area is fully covered with a water droplet after withdrawal. If this is the case, the membrane is finally mounted into the electrochemical cell.

Electroplating is done in a Teflon cell with the substrate (membrane) facing upward. There is no separate compartment for the counter electrode which is a Pt plate of about 10 cm^2, nor is there any agitation (stirring) or heating. A saturated-calomel electrode (SCE) was used as reference for the applied potential. This electrode is placed ≈7 mm above the substrate. Using a conventional potentiostat, the current is measured during electroplating at a fixed potential versus SCE, refered to as V_{SCE}. The growth in pores has been studied for Ni, Co, Cu, and Au deposits as well as for polypyrrole polymer synthesis. The following aqueous electrolytes have been used: Ni solution, 515 g/L Ni(H$_2$NSO$_3$)$_2$·4H$_2$O + 20 g/L NiCl$_2$·6H$_2$O + 20 g/L H$_3$BO$_3$; Co solution, 400 g/L CoSO$_4$·7H$_2$O + 40 g/L H$_3$BO$_3$; Au solution, 0.32 M gold(I) cyanide + 0.26 M citric acid and 0.65 M KOH (pH = 5−6); Cu solution, 125 g/L CuSO$_4$·5H$_2$O + H$_2$SO$_4$ such that pH = 1; pyrrole solution, 0.5 M pyrrole monomers (from a freshly distilled solution) + 0.1 M LiClO$_4$. Typical deposition voltages are −1.2, −1.1, −1.0, −0.2, and +0.8 V$_{SCE}$ for Ni, Co, Au, Cu, and pyrrole, respectively.

After electroplating, the membrane is inspected under an optical microscope. If the growth has been interrupted while the pores where not completely filled, areas on the membranes covered with nanowires appear black. If the pores were completely filled and growth proceeded on the whole membrane surface, a three-dimensional "bulk" film starts to cover the membrane. If this is the case, the membrane appears reflective in the case of metal deposits. These two simple observations allow one to test the degree of growth homogeneity on the membrane. In order to measure the diameter of the wires, the polycarbonate membrane is dissolved in 40 °C dichloromethane (Cl$_2$CH$_2$), rinsed in fresh dichloromethane, chloroform, and ethanol. This preparation procedure is sufficient for standard SEM work. However, high resolution images still suffer from electron-beam-induced charging effects which are caused by a residual organic (and insulating) layer on the wires. In case of metal wires, this organic coating has been removed in an oxygen plasma treatment at 100 °C.

3. Experimental Results and Discussion

3.1 Nanowires Grown in 80-nm-Wide Pores. The most comprehensive dataset has been obtained for membranes with a nominal pore diameter of d_N = 80 nm. For this reason, we initially focus our attention to these membranes. Figure 1a shows two electric current I versus time t characteristics (I−t characteristic) for the reduction of Ni^{2+} and Co^{2+} ions obtained during electrodeposition at constant applied voltage (potentio-

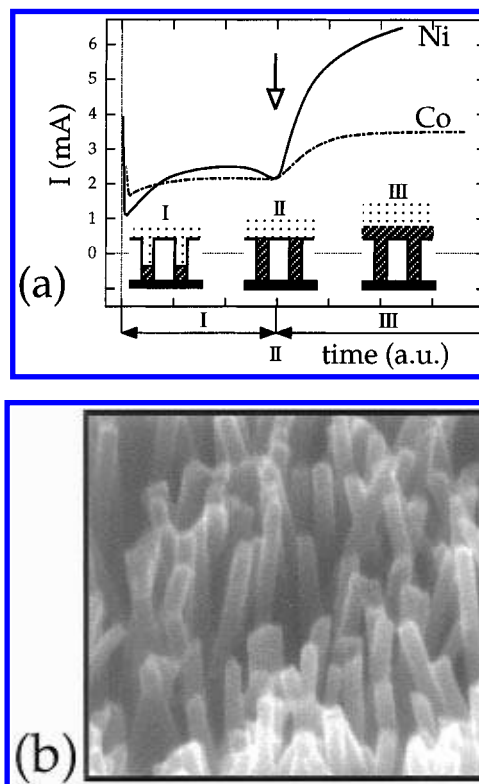**Figure 1.** (a) Electrochemical reduction current $I(t)$ as a function of time t for the potentiostatic plating of Ni and Co (−1.1 V$_{SCE}$ for Ni and −1.2 V$_{SCE}$ for Co) in pores of polycarbonate membranes with d_N = 80 nm (nominal pore diameter). The schematics display three different stages of the growth process: in region I, metal wires (hatched) grow in the pores, in region II, the pores are just completely filled (transition region to bulk growth), and in region III, growth commences over the whole membrane (diameter 6 mm). (b) SEM image of the Ni deposit obtained after dissolution of the polycarbonate membrane. Electrodeposition has been stopped in region I.

statically) on these membranes. In the same figure, two pores are schematically drawn in cross-section at three different stages of the growth process. During the first stage (left schematics labeled I) the metal (shown hatched) is growing in the pores while the reduction current takes on a value of ≈2 mA (the variation in the current will be discussed below). Growth proceeds in the pores until they are filled up to the top surface of the membrane (middle schematics). Beyond this, growth can continue in three dimensions: hemispherical caps form on top of the wires (see also Figure 2a and 4) which grow in size until coalescence on the membrane surface occurs. This is the transition region (labeled II), which starts at the position of the arrow in Figure 1a. Since the effective electrode area increases rapidly during this stage, the electrochemical current increases. In the following, the term "transition to bulk growth" will be used. Once growth proceeds on the whole membrane surface (right schematics labeled III), the current approaches an asymptotic value. This value corresponds to the current measured on a metallic electrode of the same overall area and for the same applied voltage.

Figure 1b shows an image of Ni wires after dissolution of the polycarbonate membrane obtained by scanning electron microscopy (SEM). In this example, the deposition was interrupted before the transition to bulk growth. The wires, observed in Figure 1b, are oriented in a wide range of directions. This is not an artifact produced by the dissolution of the membrane, which could be suggested, because during dissolution and drying mechanical forces tear on the wires. It is a property intrinsic to commercial screen membranes. The pores

Template Synthesis of Nanowires

J. Phys. Chem. B, Vol. 101, No. 28, 1997 **5499**

in these membranes are not aligned parallel but have a considerable angular distribution of ±34° (Poretics[10] production selection guide). For this reason, the length of the pores, measured through the membrane, is not constant. Hence, even if the electrochemical deposition would proceed at an exactly constant rate, the instant of complete pore filling would still vary among different pores. This is one reason (of fundamental origin) that broadens the "sharp" transition to 3D bulk growth observed in the $I-t$ characteristic. Another is inhomogeneous growth: if some of the pores are initially poorly wetted, the number of pores in which electrodeposition occurs can increase with time. This (1) results in a current, which gradually increases, and (2) leads to a considerable smearing out of the transition to bulk growth (not shown). A sharp transition, as the one seen in Figure 1a (and following figures) is a good criterion for homogeneous growth.

In Figure 1a a strong increase of the current is observed when the deposition starts to change from growth in pores to growth on the whole surface of the membrane. To a first approximation, this increase may be related to the changing effective electrode area. The membranes have a typical porosity of ≈5% (using an effective electrochemical pore diameter, defined later), so that the electrode area increases by at least an order of magnitude. However, the observed current only increases by a factor 3−4 for Ni and ≈2 for Co. The observed reduced current increase at the transition is attributed to partial mass transport limitation (convection and diffusion). Though high ionic concentrations ≈1 M are used for all plating solutions, electroplating on the whole membrane surface is not ideal; i.e., it does not only depend on electrode parameters (applied voltage and electrode area), but also to a certain degree on the transport of ions from the solution reservoir to the electrode region, where the ionic concentration is (partly) depleted. In order to test this conjecture, we applied electrolytes with a diluted concentration of Cu^{2+} ions. For low concentrations (1−10 mM) the current rise, which is observed at the transition to bulk growth in highly concentrated electrolytes, completely disappears. The changing electrode area at the transition does not change the electric current, because it is limited by mass transport in the bulk electrolyte. Hence, we can conclude that the smaller electric current rise at the transition to bulk growth for Co with respect to Ni seen in Figure 1a demonstrates that mass transport limitation is more important for Co as compared to Ni. It is important to emphasize that highly concentrated electrolytes are a prerequisite for monitoring the growth process with the aid of the $I-t$ characteristic.

While Figure 1b displays a SEM image of Ni wires obtained from a growth run, which was stopped before the transition to bulk growth, Figure 2 corresponds to situations at the point of transition (Figure 2a) and long thereafter (Figure 2b), when the metallic deposit covers the whole membrane. On some of the wires in Figure 2a small hemispherical caps have already been formed.

In the following, the apparent wire diameter d_a deduced from SEM images (similar to Figure 1b) of Ni and Co wires will be compared to the electrochemically derived effective wire diameter d_e. First, the pore diameter and density of empty polycarbonate membranes are studied with SEM. In order to render electron microscopy possible, the membranes have been coated with a thin (10 nm) conducting layer. We measure a pore diameter of $d_s = 78 \pm 18$ nm (d_s = "surface" diameter) and a pore density of $n_p = 7 \times 10^8$ cm^{-2} in reasonable agreement to values specified by the manufacturer ($d_N = 80$ nm and $n_p = 4 \cdot 10^8$ cm^{-2}). Since the growing area is predetermined by the adhesive sticker (diameter $D = 6$ mm),
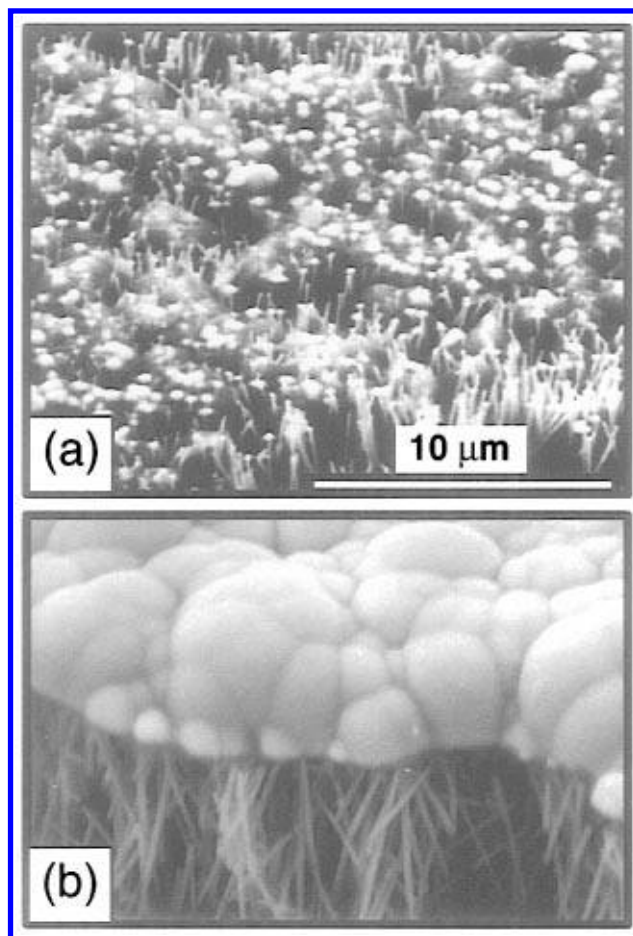

Figure 2. SEM images (equal magnification) of the Ni deposit plated into $d_N = 80$ nm porous membranes obtained after dissolution of the polycarbonate membrane. Electrodeposition has been stopped at the transition to bulk growth (region II in Figure 1a) and long afterwards (region III) for (a) and (b), respectively.

the total number of pores N_p is known: $N_p = n_p D^2 \pi/4$. The volume V_p of one completely filled pore, assuming an effective electrochemical diameter d_e, is given by $V_p = L d_e^2 \pi/4$, where $L = 6$ μm is the thickness of the membrane (approximate for the maximum length of the wires). Using the molar volume V_M of Ni or Co (almost identical), the total charge needed to fill all the pores up to the membrane surface is $Q = zFN_pV_p/V_M$, where $z = 2$ for the divalent Co^{2+} and Ni^{2+} ions and F is the Faraday constant. This charge Q is approximated by the experimentally obtained charge Q_t that has been transferred in the cell from the start of growth up to the point of transition to bulk growth (Q_t is refered to as the transition charge). Here, a 100% current efficiency is assumed. This assumption has carefully been studied and confirmed for the Co bath, which is similar in concentration than the other applied electrolytes.[18] Since the transition charge Q_t for many runs of Co and Ni deposits show no difference within the accuracy of the measurements, a 100% current efficiency for the Ni bath is justified as well. From ≈50 samples (Ni and Co deposits), where the growth covered the whole exposed area, we obtain $Q_t = 0.7 \pm 0.13$ C. Using this value, an effective electrochemical diameter $d_e = 161 \pm 19$ nm is deduced (the error given includes the uncertainty of the wire length). Similarly, from SEM images we obtain an apparent average diameter $d_a = 180 \pm 40$ nm. These values for the diameter are in good agreement with the result of Chlebny et al.[17] who studied the diameter of similar wires with transmission electron microscopy and found a value of $d_a = 164 \pm 10$ nm. Both from electron microscopy images of nanowires and electrochemically transferred charge, a consider-
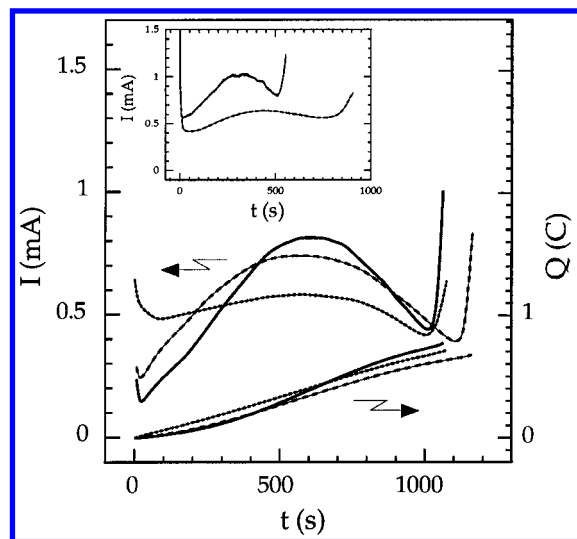
5500 *J. Phys. Chem. B, Vol. 101, No. 28, 1997*

Schönenberger et al.

Figure 3. Three examples of the electrochemical reduction current $I(t)$ (charge Q) versus time t for potentiostatic Ni growth ($U = -1.0$ V_{SCE}) in pores of polycarbonate membranes with $d_N = 80$ nm. Inset: $I(t)$ for Cu (solid curve) and Co (dashed curve) at $U = -0.1$ and -1.1 V_{SCE}, respectively.

Figure 4. SEM images of Ni wires grown in $d_N = 80$ nm membranes after dissolution of the membrane. The growth was stopped after the transition to bulk growth during which hemispherical caps were formed. The wires have a length of $\approx 6\ \mu$m and an apparent diameter of $100-280$ nm.

able (factor 2) larger wire diameter is found as compared to the nominal pore diameter d_N. Data obtained for Cu and Au deposition (not shown) are in full agreement with the Co and Ni data.

In region I (Figure 1a) where electroplating proceeds in the pores, the observed electrochemical current is not constant. Details of the $I-t$ characteristic during this growing period are shown in Figure 3. Three $I-t$ curves representative for Ni deposition at $U = -1.0$ V_{SCE} together with the integrated current, i.e., the charge $Q(t)$, are displayed. Growth proceeds in the pores up to $t \approx 1000-1200$ s when the rapid current increase signals the transition to bulk growth. For these examples, the transition charges are 0.65, 0.67, and 0.75 C, which are values in agreement with the average of 0.7 ± 0.13 C. Starting growth in the pores, the current first increases with time, approaches a maximum after $\approx 1/2$ of the period needed to fill the pores up to the top membrane surface, and then starts to decrease significantly before the transition to bulk growth. In general, the current maximum is found to be more pronounced the sharper the current rises at the point of transition, which is the case if almost all wires approach the top surface of the membranes simultaneously (ideal case). To a first approximation, the length l of the wires can be assumed to be proportional to the time t, that has elapsed after growth was initiated. Hence, we observe a deposition current, which can be up to factor of 6 larger than the initial current, when the wires have been grown to a length $\approx 1/2$ of the total pore length of $L \approx 6\ \mu$m. The decreasing reduction current with progressive growth is quite unexpected: the electrochemical current is determined by the applied voltage and, if mass transport is a limitation, by the diffusion of ions. Since the reference electrode is located in the bulk electrolyte (reservoir) above the membrane, there may be a voltage drop along the electrolyte in the pores which would result in a reduced electrochemical current. With progressive growth, this voltage drop should decrease, however, since the wires are approaching the reservoir. Hence, the current is predicted to increase. A similar conclusion is reached if mass transport limitation is considered. As a first-order approximation, one may assume a constant ion concentration in the electrolyte (reservoir) above the pores. The concentration gradient, which determines the diffusion current, increases if the wires approach the top surface of the membrane, so that
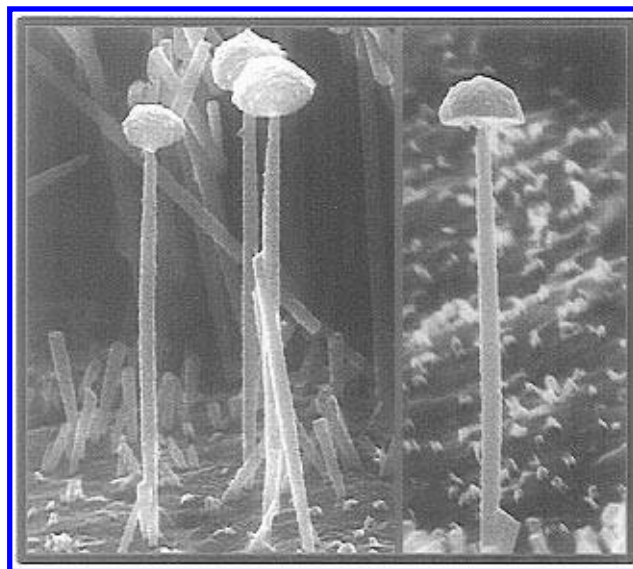
the diffusion current increases as well. The surprising current drop in the $I-t$ behavior is also observed for all the other electrochemical systems studied (Ni, Co, Au, Cu, and pyrrole). These systems correspond to a wide range of deposition voltages ranging from -1.3 to $+0.8$ V_{SCE}. As an example, the inset of Figure 3 shows $I-t$ curves for Cu, grown at $U = -0.1_{SCE}$ (solid line), and for Co, grown at $U = -1.1$ V_{SCE} (dashed line). In both cases, clear maxima are observed (less pronounced for Co, in general). In addition to using different solutions, the deposition time for pore filling was also varied by changing the applied voltage. For the range $U = -1.3$ to -1.0 V_{SCE}, used for Ni deposition, which corresponds to $120-1200$ s, the maximum was always clearly observable.

Apart from diffusion and migration, the electrochemical current is also proportional to the electrode area. The current maximum is due to an increased wire diameter in the middle section of the nanowires, as will be demonstrated. Figure 4 shows high-resolution SEM images of Ni wires viewed from a direction almost perpendicular to the wires. These wires originated from a membrane which was electroplated a short instant beyond the point of transition. The hemispherical caps on the top of the wires develop just after the pores are completely filled. In Figure 4, the wire diameter is observed to be larger in the middle than at the bottom (where growth started first) and top immediately underneath the caps. This effect is even more pronounced in two extreme examples displayed in Figure 5. In the left image the bottom and top 2 μm of the same wire are shown. The diameters are 100 and 75 nm close to the bottom and top and 210 nm around the middle section. In the right image the diameters are ≈ 100 nm close to the top and bottom and 240 nm in the middle. The wires are observed to be up to a factor of 2.5 wider in the middle than at the base or top end. This increase in diameter, which amounts to a factor of ≈ 6 increase in area, is consistent with the $I-t$ behavior of Figure 3. The observed dimensions are also in agreement with the average of the effective electrochemical pore diameter of about 160 nm.

There are two possible reasons for the increased diameter. First, the pores may not be cylindrical (but wider inside), or second, the pores widen during growth. This latter scenario can originate during metal deposition, if the metal not only
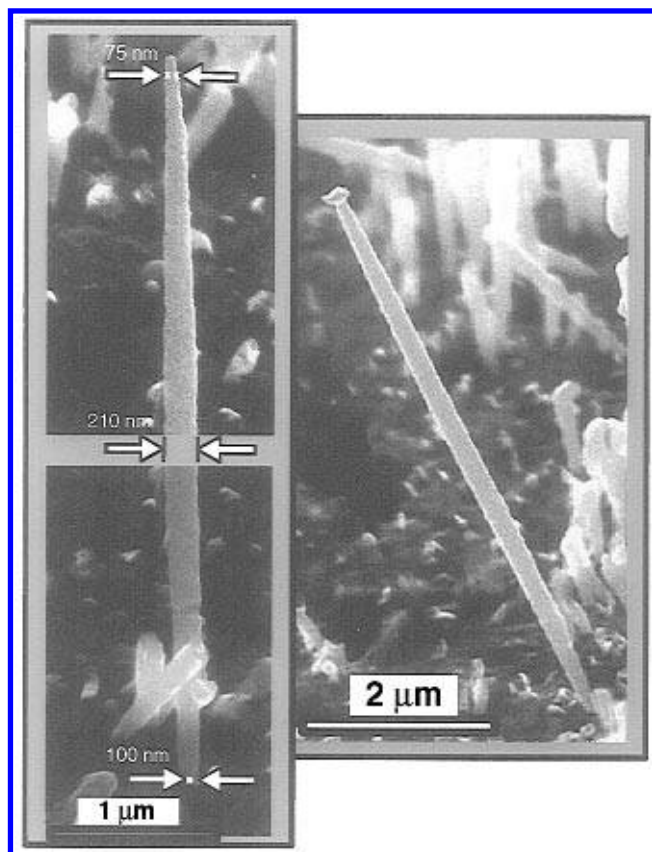
Template Synthesis of Nanowires

J. Phys. Chem. B, Vol. 101, No. 28, 1997 **5501**

Figure 5. SEM images of Ni wires grown in $d_N = 80$ nm membranes after dissolution of the membrane. The growth was stopped immediately at the transition to bulk growth. The two images to the left display the top and bottom 2 μm of the same wire (total length $\approx$6 μm). Note the remarkably increased diameter in the middle section of the wires.

grows strictly along the direction of the pore axis but also to a certain degree radially, exerting pressure onto the polycarbonate membrane which causes a widening of the pores. For this scenario a decreasing wire diameter with progressive growth would be difficult to understand, since the mechanical strain would relax much easier near the membrane surface. As a test, polymeric wires were also potentiostatically grown in the these pores. Since the polymer is expected to have mechanical properties more similar to the template material (all "soft matter"), a widening imposed by the growing wires is not expected in this case. Figure 6 shows two SEM images of the top part of pyrrole polymer wires after dissolution of the polycarbonate membrane. Even though the image contrast is much poorer here, one can clearly see that the wires narrow at the top (see arrows). In the right image of Figure 6 the border of a wire is highlighted by dashed lines. This wire has a diameter of 93 nm at the top and 250 nm in middle section, in agreement with results for metal wires.

We thus can conclude that the pores themselves are in general not cylindrical with a constant cross-section but are rather *cigarlike*. For the analyzed pores with a nominal diameter of $d_N = 80$ nm, the middle section of the pores is wider by up to a factor of 3. This is not in contradiction to SEM studies, in which the membrane surface and hence the pore diameter just at the surface are studied. This apparent diameter is comparable to the nominal one.

The observed current maxima in Figure 3 directly reflect the shape of the pores. We mention that a similar maximum is observed in case of $d_N = 50$ and $d_N = 200$ nm membranes. This maximum is also (and with similar intensity) present in pores of membranes obtained from different suppliers (i.e.,
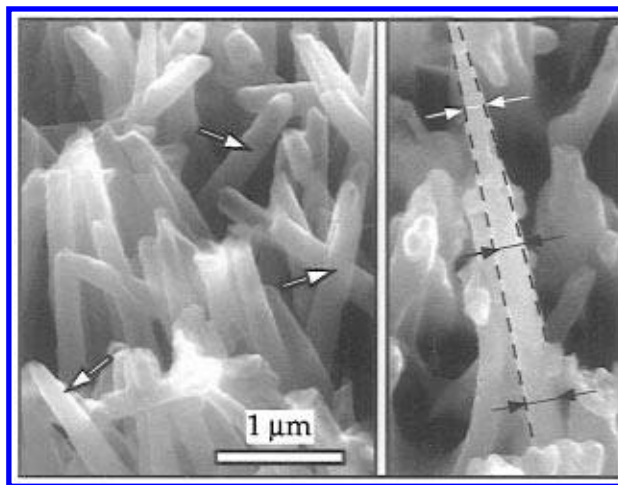

Figure 6. SEM images of polypyrrole fibrils potentiostatically grown in $d_N = 80$ nm membranes after dissolution (in part) of the membrane. Note that the polymeric wires are thinner at their end (e.g., arrows on the left image). In the right image (identical magnification), the variation of the diameter d along the wire is emphasized with dashed lines that follow the border of the wire. In this case $d \approx 130$ nm at the top end and $d \approx 250$ nm in the middle section. The bottom section of the wire cannot be seen here.

Poretics, Nuclepore, and Millipore). For smaller diameters, however, the $I-t$ dependence is different as will be discussed below.

3.2. Nanowires Grown in 10- and 30-nm-Wide Pores. Figures 7 and 8 show representative SEM images of Ni wires grown in polycarbonate membranes with nominal pore diameters of $d_N = 30$ and $d_N = 10$ nm, respectively (pore density also $n_p \approx 7 \times 10^8$ cm^{-2}). In Figure 7, two wires are shown over their whole length ($\approx$5.5$-$6 μm). These images serve to check whether size variations along the wires exist, similar to the previous observation for $d_N = 80$ nm. Although there are variations in the diameter, partially due to the granular structure of the wires, no systematic dependence can be observed, except for the very end of the wires: for wires which were grown to their full length given by the membrane thickness ($L \approx 6$ μm), the wires are seen to systematically narrow at the very end over the last few 100 nm. Three examples are indicated in Figure 7 by arrows. This narrowing suggests that the inner pore diameter at the top and bottom surface of the membrane is approximately in agreement with d_N but is considerably wider inside the membrane. This is similar to the $d_N = 80$ nm case, except that the thinner pores now widen over a shorter distance measured from the membrane surface. From figures similar to Figure 7 and 8, the average apparent (by SEM) diameter of the wires is found to be $d_a = 80 \pm 20$ nm ($d_N = 30$ nm) and $d_a = 50 \pm 18$ nm ($d_N = 10$ nm). An effective electrochemical diameter for the $d_N = 10$, 30 nm membranes is derived from the transition charge Q_t obtained from $I-t$ curves, which will be discussed below.

The results for all three membranes are summarized in Table 1. The data for the wire diameters measured with TEM are taken from ref 17. A remarkably good agreement between the electrochemically derived diameter d_e and the apparent diameter d_a measured with TEM is evident. In contrast, the data obtained from SEM images, systematically overestimate the diameter of the wires by $\approx$14$-$23 nm, which presumable is related to the reduced resolution of SEM compared to TEM.

Since we have demonstrated before that the wires are true replicas of the pores (except for the granular structure of the wires), we may state that the pore diameters (averaged over the whole pore length) are factors of $\approx$2, 2.1, and 3.6 wider
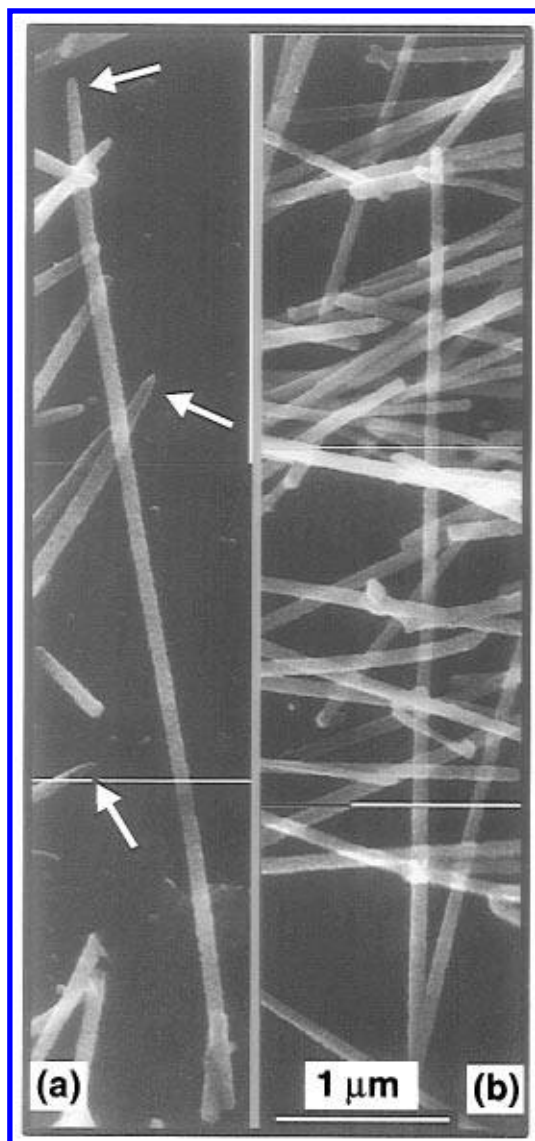
Figure 7. SEM images of Ni wires grown in $d_N = 30$ nm membranes after dissolution of the membrane. The arrows point to wires where the narrower wire cross-section at the end regions can be seen best.
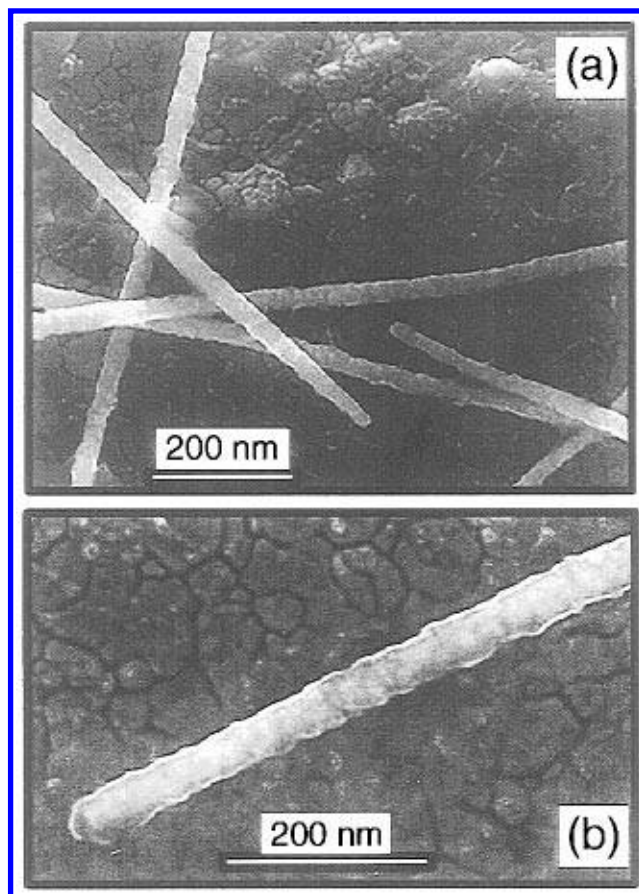

Figure 8. SEM images of Ni wires grown in $d_N = 10$ nm membranes after dissolution of the membrane. Note, that the roughness along the wire etch amounts to 4 nm, only. It is pressumably caused by the granularity of the metal.

TABLE 1: Data for Wires Grown in Polycarbonate Membranes with a Nominal Pore Diameter d_N[a]

d_N, nm	Q_t, C	d_e, nm	d_a, nm (SEM)	d_a, nm (TEM) from ref 17
80	0.7 ± 0.13	161 ± 19	180 ± 40	164 ± 10
30	0.11 ± 0.02	63 ± 8	80 ± 20	57 ± 3
10	0.035 ± 0.008	36 ± 6	50 ± 18	36 ± 3

[a] Q_t is the electrochemical charge needed to fill all pores over a membrane area with diameter 6 mm. d_e is the average electrochemical wire diameter obtained from Q_t, and d_a (SEM/TEM) is the average diameter derived from SEM and TEM (from ref 17) images of these wires.

than specified. With respect to the effective wire cross-section, the area is on average up to a factor of 10 larger than what would be assumed if the nominal values were used. This can drastically influence physical parameters derived from measurements on these wires, e.g., ref 12.

Finally, we discuss the $I-t$ characteristics measured for membranes with $d_N = 30$ and 10 nm. Figure 9a displays three representative $d_N = 30$ nm $I-t$ curves for Ni growth at $U = -1.2$ V_{SCE} (curves labeled a, b) and $U = -1.15$ V_{SCE} (curve labeled c). Curve c is rescaled so that the point of transition to bulk growth approximately coincides with the other two curves ($t \approx 220-230$ s) in the figure. Experimentally $I(t)$ was $\approx 2\times$ smaller and the time scale $\approx 2\times$ longer. The transition charge Q_t for the three curves are 90, 100, 125 mC with an average (over many curves) of $Q_t = 0.11 \pm 0.02$ C (see Table 1).

Figure 9b displays $I-t$ curves for $d_N = 10$ nm. The solid curves (a−c) correspond to Ni grown at $U = -1.2$ V_{SCE}, while the dashed curve (d) is an example for Co growth at $U = -1.06$ V_{SCE}. The top two curves (a, b) represent examples in which the largest currents have been observed for these membranes, corresponding to a complete filling of all pores. Q_t are 40 and 45 mC (average 35 ± 8 mC). $I-t$ curves with smaller currents, similar to the two bottom curves (c, d) of Figure 9b, are often

measured in case of membranes with the smallest pores. Similarly, the relative surface coverage of filled pores is often found to be reduced for these kind of membranes. This demonstrates the difficulty in getting all pores wetted by water prior to electrodeposition.

The $I-t$ characteristics in Figure 9a show some structure: there is a current rise during the initial growth phase and similar to the $d_N = 80$ nm membranes a drop just before the pore filling is completed at the point of transition to bulk growth. These two observations are in agreement with the geometry of the wires: the wires are found to be narrow close to the bottom and top end (discussed above). The $I-t$ curves in Figure 9 seem to develop a current minimum after $\approx ^1/_2$ of the maximum wire length, which geometrically would correspond to a narrowing of the wires in the middle section. Though this narrowing cannot be supported by SEM images, it is thought to be related to the average geometry of the wires (expressed in diameter, the effect is expected to be small).
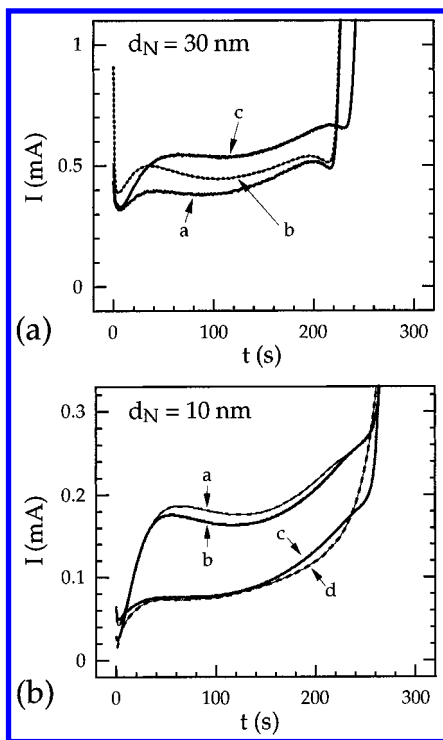
Template Synthesis of Nanowires

J. Phys. Chem. B, Vol. 101, No. 28, 1997 **5503**

Figure 9. Electrochemical reduction current $I(t)$ versus time t for potentiostatic metal deposition in polycarbonate membranes with (a) $d_N = 30$ nm and (b) $d_N = 10$ nm pores. All curves correspond to Ni plating, except for the dashed one in (b), which corresponds to Co.

Comparing the $I-t$ characteristics for all three pore diameters, there is, in addition to the geometric dependence, a significant difference: for the thinner two pore diameters, $I(t)$ has the tendency to increase with time. This increase is very pronounced for $d_N = 10$ nm. Here, the current has a gradual increasing component, because of which the transition to bulk growth can hardly be discerned. From the discussion of Figure 1a, we know that mass transport is more a limiting factor for Co than for Ni growth. The dashed curve (d) in Figure 9b is an example for Co growth in the narrowest pores. Apart from the initial rise and plateau, there is a smooth and gradual increase of $I(t)$, which extends beyond the transition to bulk growth. The transition point cannot be determined unambiguously anymore. We think that the increasing current is caused by mass-transport limitation. The current increases close to the point of transition because the wire approaches the top membrane surface and, therefore, also the large electrolyte reservoir, in which the ion concentration is approximately constant. That the current is increasingly controlled by diffusion for smaller pore diameters is only consistent if the diffusion coefficient D for the active ion species is pore-size dependent. Measurements of D versus d_N, discussed in the next section, support this conclusion.

3.3. Size Dependence for the Diffusion of Ions in Pores. In this section measurements of the diffusion coefficient for the electroactive electrolyte ions in the restricted geometry of the pores are discussed. There are two standard approaches to determine the diffusion coefficient D: First, there is the rotating disk method for which the limiting current I_{lim} is proportional to $D^{3/2}\omega^{1/2}$, where ω is the angular rotation speed of the electrode. Second, D can be obtained from the initial time dependence of the limiting current, which in one dimension is given by $I(t) = zFc^*A/(D\pi t)^{1/2}$, where A is the active electrode area and c^* the bulk ion concentration present before plating starts. Integration yields for the transferred charge $Q(t) = 2zFc^*A$ $(D/\pi)^{1/2}t^{1/2}$. Both methods relate the diffusion coefficient to the limiting current I_{lim}, for which the ion concentration
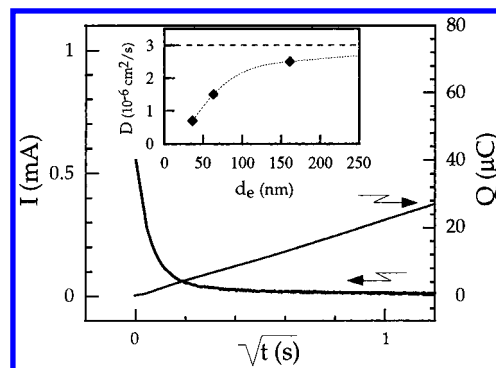

Figure 10. Time dependence of the electrochemical reduction current $I(t)$ (charge $Q(t)$) of diluted Cu^{2+} measured in $d_N = 30$ nm pores. The curves are drawn with respect to $t^{1/2}$ to emphasize the one-dimensional diffusion behavior of the limiting current. Inset: Diffusion coefficient D (squares) obtained from a set of $Q(t)$ dependences as a function of the "effective" electrochemical pore diameter d_e. The dashed horizontal line is shown as a reference. It corresponds to $D = 3.6 \times 10^{-6}$ cm^2/s, measured for a flat electrode using the rotating disk method. The dotted line is a guide to the eye.

at the electrode surface is assumed to be zero. For the standard highly concentrated electrolytes used in our study, the current is only partially mass-transport limited, since no limiting plateau has developed for the applied voltages. In order to realize a situation in which the electric current is equal to the limiting current during electrodeposition in the pores, another electrolyte is used. This electrolyte is based on the standard Co electrolyte (concentration 1.2 M) to which $1-10$ g/L CuSO$_4$·7H$_2$O is added. This amounts to a molar concentration of $3-30$ mM. Since the equilibrium potential for $Co^{2+} + 2e \rightleftharpoons Co$ (-0.57 V$_{SCE}$) is much more negative than that for $Cu^{2+} + 2e \rightleftharpoons Cu$ ($+0.07$ V$_{SCE}$), it is possible to reduce Cu^{2+} in the range of the limiting current plateau for Cu deposition without depositing Co. This electrolyte allows one to measure the diffusion coefficient of the diluted component Cu^{2+}, which is present in an environment of highly concentrated Co^{2+} ions. We assume that the diffusion coefficient obtained for the Cu^{2+} ions represents to a first approximation the one for the Co^{2+} ions. This is justified because of the presence of the highly concentrated Co^{2+} ions, so that the Cu^{2+} ions experience a similar environment as the Co^{2+} ions, at least with regard to electrostatics.

The rotating disk method is only applicable for flat electrodes, since it relies on the shape of the flow profile of the electrolyte. Therefore, this method cannot be used for the pores as substrate. We used it, however, to obtain a reference value for a flat Cu electrode. We derive $D = 3 \times 10^{-6}$ cm^2/s. The procedure used for pores is the following: starting with the standard Cu bath (high concentration), the pores are filled at $U = -0.15$ V$_{SCE}$ during 50 s, which corresponds to a grown wire length of ≈ 1 μm. Next, the membrane is flushed with deionized water before the Co/Cu electrolyte is added. The initial $I(t)$ characteristic is measured at $U = -0.5$ V$_{SCE}$ during the first few seconds. This $I(t)$ dependence is used to estimate the diffusion coefficient. The membrane is flushed with water again and the original highly concentrated Cu electrolyte is applied again. Electroplating proceeds in this solution up to the point of transition to bulk growth. The current is also monitored during plating by using the standard Cu bath. This allows one to derive the transition charge Q_t and, therefore, to verify whether all pores have been filled.

Figure 10 shows a representative $I(t)$ curve and the derived charge $Q(t)$ for Cu deposition in the mixed Co/Cu bath for a $d_N = 30$ nm membrane. Note, that the curves are displayed versus $t^{1/2}$ in order to emphasize the proportionality of Q with $t^{1/2}$. The diffusion coefficient D can be obtained from the slope of the Q

vs $t^{1/2}$ curve ($Q = 2zFAc^*(D/\pi)t^{1/2}$), provided the true electrode area A is known for which the pore diameter d and the pore density are needed. For d we use the average electrochemically determined diameter d_e, previously derived and tabulated in Table 1. The following values are obtained: $D \simeq 2.5, 1.5,$ and 0.7×10^{-6} cm^2/s for $d = 80, 30,$ and 10 nm, respectively. In the inset of Figure 10, the diffusion coefficient is shown relative to d_e. We note that the value for the largest pores is consistent with the one obtained for the macroscopic electrode by the rotating disk method (3×10^{-6} cm^2/s). The diffusion coefficient decreases by approximately a factor of 3 for the smallest pores studied.

Since the electrochemical current for growth in pores is most strongly dependent on diffusion in the case of the narrowest pores, we estimate the stationary limiting current at the beginning of metal deposition for $d_N = 10$ nm pores: this limiting current for one single pore is given by $I_p \approx zFA_pc^*D/L$, where A_p is the cross-sectional area of the pore. Using $d_e = 36$ nm, $c^* = 1.2$ M, $D = 0.7 \times 10^{-6}$ cm^2/s, and $L = 6$ μm, one obtains $I_p = 2.7$ pA. The total current is obtained by multiplying with the number of pores and is found to be $I_{lim} \simeq 0.5$ mA. The measured current of ≈ 0.2 mA (Figure 9b) is already close to the limiting current, demonstrating that diffusion has to be considered in the interpretation of the $I-t$ curves in the case of the narrower pores.

In the following, we speculate on possible mechanism that may influence the ion transport in the confined geometry. Size effects can occur when the medium (here the electrolyte) is restricted to a volume of size comparable (in at least one dimension) to a characteristic length scale of the medium. For an electrolyte, important length scales are the mean distance between ions d_{nn} and the Debye–Hückel screening length d_{DH}. For the standard Co solution with a ion concentration of 1.2 M, we estimate $d_{nn} = 1.25$ nm and $d_{DH} = 0.4$ nm, values that are still much smaller than the effective pore diameter. Therefore, if ions were to adsorb on the pore walls, the electrostatics of the electrolyte within the pores is not expected to change, since the extend of the double layer (expressed by the Debye–Hückel screening length) is very small. If an ion happens to reach the pore wall during its random walk it may stay there for a longer period, if an attractive ion–polycarbonate interaction is present. This would reduce the effective diffusion coefficient D. Because of the high ion concentration, however, only a small fraction of ions can participate in such a process. The diffusion coefficient D can, however, also be reduced as a result of the changing properties of the carrier medium (water). According to Einstein, $D = kT/6\pi\eta r$ for a rigid particle of radius r in a solution with viscosity η. In our case, r has to be replaced by an effective ion radius. Taking $D = 3 \times 10^{-6}$ cm^2/s and $\eta = 10^{-3}$ kg/m s (for water at 20 °C) yields a radius of $r = 0.73$ nm. Though this formula is certainly not valid in this situation, the derived effective radius is a reasonable measure of the ion size including its hydration shell. Since this effective radius is much smaller than the pore diameter, this parameter is most likely not changed for the different pore dimensions. We think that the diffusion coefficient is pore-size-dependent because of the (effective) viscosity η for water, which increases significantly for smaller pores. This observation may be related to the PVP (polyvinylpyrrolidone) which is applied to the membrane as a wetting agent by the manufacturer. According to the D versus d_e dependence, shown in the inset of Figure 10, the diffusion coefficient extrapolates to zero for an effective diameter of $\approx 10-20$ nm. This is in contradiction with the finding that very narrow nanopores (diameter $\lesssim 10$ nm) in Al$_2$O$_3$ membrane can still be filled by using similar electrolytes. This remark supports the hypothesis that PVP adsorbed on the pore walls may be responsible for the observed pore size dependence of the diffusion coefficient.

3.4. Origin of the Widened Pore Diameter. This final paragraph is devoted to the question of why the pores are wider inside the membrane than close to the surface. We speculate that this effect is a consequence of the ion impact during "exposure". Each pore is formed by a single highly energetic ion traversing the membrane. The direct impact interaction produces a damage zone along the ion track (damage track).[19] The membrane is then etched in a solution with a high selectivity for damage tracks; i.e., the etching rate for the damaged zone is much larger than for the undamaged material. For polycarbonate, this selectivity is found to be ≈ 400.[20] During this process, a physical hole is opened in the membrane. Since etching proceeds from the top and bottom surface, the pore is expected to assume a shape with a thinner middle cross section. This is just the opposite of what is observed in our work. However, one has to keep in mind that the (primary) damage zone is localized within a very narrow region. A typical damage diameter is 10 nm.[21] Once the pores are open, they widen with progressive etching time, ideally homogeneously, in which case cylindrical holes will develop. We think that this is not the case, at least for the smaller pore diameters $d \lesssim 200$ nm, because of a secondary effect, which also modifies the membrane (polycarbonate). Besides the primary damage, caused by the ion impact, a large number of secondary electrons are generated at any point along the track (electronic collision cascade).[19] These electrons themselves have sufficient energy (already a few electron volts are enough) to interact destructively with the polymer membrane by cleaving chemical bonds, for example.[22] The resulting smaller polymeric fragments are etched more easily than the original polymer, and since the range of secondary electrons is large (up to ≈ 1 μm), the etch rate can also be enhanced at positions away from the track center. This effect is very well-known in electron beam lithography (e-beam lithography).[23] Here, a focused medium energy electron beam ($\approx 10-100$ keV) is used to expose a resist, which most often is PMMA with a molecular weight of ≈ 100K. In the developing step (etching), the exposed material is dissolved. A fundamental problem in e-beam lithography is the fact that also secondary electrons expose the resist, often they even dominate the exposure. Since secondary electrons can penetrate the polymer over rather long distances, the resist is effectively exposed laterally away from the position of the primary beam. This effect has been termed "proximity effect" in e-beam lithography. We propose that the pore widening is a consequence of proximity exposure. This suggestion allows one to understand why etched pores are in general wider inside than at the top and bottom end of the membrane. Let us assume that the secondary electrons are generated isotropically at each point along the ion track in the membrane. Any point in the vicinity of the track, but sufficiently inside the membrane, receives exposure from secondary electrons generated above *and* below this point. This is different for a point close to the membrane surface. On the top surface, for example, impinging secondary electrons can only originate from below this point, since the impacting ion moves through vacuum above. For this reason, proximity exposure is reduced by approximately a factor of 2 close to the membrane surface. If etched, the pore will develop a smaller diameter at the top and bottom of the membrane compared to regions inside.

4. Summary

The time (t) dependence of the current I during electroplating (potentiostatic mode) in nanopores of commercially available

Template Synthesis of Nanowires

J. Phys. Chem. B, Vol. 101, No. 28, 1997 **5505**

polycarbonate screen membranes with nominal pore diameters of $d_N = 200, 80, 30,$ and 10 nm is studied, as well as the geometric shape of the deposits (nanowires), which are Ni, Co, Cu, and Au metallic deposits or conducting polymers obtained by the electropolymerization of pyrrole. From scanning electron microscopy (SEM) images of nanowires, obtained after dissolution of the membrane, the apparent wire diameter in general exceeds the nominal pore diameter by up to a factor of 3. The wires are not uniform in width; however, they are wider in the middle as compared to the top and bottom (end) sections. The top and bottom region, where the diameter assumes a value in reasonable agreement with d_N specified by the manufacturer, correspond to regions close to the membrane surface. This wire widening is most pronounced for wires obtained from $d_N = 80$ nm membranes. The nonuniformity of the wire diameters is reflected in the $I(t)$ characteristic. From the charge Q, transferred during electroplating wires in the pores, an average (electrochemical) wire diameter can be deduced, which again is larger than d_N, in good agreement with diameters observed by SEM. It is argued that the wires are a "perfect" replica of the pores, so that the pores themselves are *not cylindrical*, in general. We think that the pores are wider inside than close to the membrane surface, because of proximity exposure by electrons that are generated in the secondary electron cascade caused by the impact of the high energy particle during nuclear track formation. For thinner pores ($d_N = 30$ nm, in particular for $d_N = 10$ nm) a gradual increase of the electrochemical current is measured, if the growing metal wires (in the pores) approach the membrane surface (and therefore, also, the electrolyte reservoir). This effect is attributed to mass transport limitations in the pores, which are more significant for narrower wires than for wider ones. Hence, the effective diffusion coefficient D is pore-size-dependent. The measured diffusion coefficient D drops from 2.5 for $d_N = 80$ to 0.7×10^{-6} cm^2/s for $d_N = 10$ nm, while $D = 3 \times 10^{-6}$ cm^2/s for a macroscopic electrode. It is speculated that PVP polymer, which is adsorbed in the pores as a wetting agent by the manufacturer, increases the effective viscosity of water.

References and Notes

(1) For a review, see: (a) Martin, C. R. *Science* **1994**, *266*, 196. (b) Brumlik, C. J.; Menon, V. P.; Martin, C. R. *J. Mater. Res.* **1994**, *9*, 1174.

(2) Possin, G. E. *Rev. Sci. Instrum.* **1970**, *41*, 772.

(3) Williams, W. D.; Giordano, N. *Rev. Sci. Instrum.* **1984**, *55*, 410.

(4) Penner, R. M.; Martin, C. R. *J. Electrochem. Soc.* **1986**, *133*, 2206.

(5) Huber, C. A.; Huber, T. E.; Sadoqi, M.; Lubin, J. A.; Manalis, S.; Prater, C. B. *Science* **1994**, *263*, 800.

(6) Furneaux, R. C.; Rigby, W. R.; Davidson, A. P. *Nature* **1989**, *337*, 147.

(7) Fleisher, R. L.; Price, P. B.; Walker, R. M. *Nuclear Tracks in Solids*; Univ. of California Press: Berkley, 1975.

(8) Tonucci, R. J.; Justus, B. L.; Campillo, A. J.; Ford, C. E. *Science* **1992**, *258*, 783.

(9) Wu, Chun-Guey; Bein, Thomas *Science* **1994**, *264*, 1757.

(10) Alumite membranes are available under the trade name Anopore from, e.g., Whatman Laboratory Division, Clifton, NJ, and polycarbonate track-etched membranes are available from, e.g., Nuclepore Corp., Pleasanton, CA, or Poretics Corporation, Livermore, CA.

(11) Kawai, S.; Ueda, R. *J. Electrochem. Soc.* **1975**, *121*, 32. Tsuya, N.; Tokushima, T.; Shiraki, M.; Wakui, Y.; Saito, Y.; Hayano, S.; Furugori, A.; Tanaka, M. *IEEE Trans. Magn.* **1986**, *MAG-22*, 1140. Arai, K. I.; Kang, H. K.; Ishiyama, K. *IEEE Trans. Magn.* **1991**, *MAG-27*, 4906. Daimon, H.; Kitakami, O. *J. Appl. Phys.* **1993**, *73*, 5391.

(12) Cai, Z.; Martin, C. R. *J. Am. Chem. Soc.* **1989**, *111*, 4138. van Dyke, L. S.; Martin, C. R. *Synthetic Metals* **1990**, *36*, 275; *Langmuir* **1990**, *6*, 1118. Martin, C. R.; Van Dyke, L. S.; Cai, Z.; Liang, W. *J. Am. Chem. Soc.* **1990**, *112*, 8976. Granström, M.; Inganäs, O. *Synthetic Metals* **1993**, *55–57*, 460. Granström, M.; Inganäs, O. *Polymer* **1995**, *36*, 2867.

(13) Blondel, A.; Meier, J. P.; Doudin, B.; Ansermet, J.-Ph. *Appl. Phys. Lett.* **1994**, *65*, 3019. Piraux, L.; George, J. M.; Despres, J. F.; Leroy, C.; Ferain, E.; Legras, R.; Ounadjela, K.; Fert, A. *Appl. Phys. Lett.* **1994**, *65*, 2484.

(14) Koopal, C. G. J.; de Ruiter, B.; Nolte, R. J. M. *J. Chem. Soc., Chem. Commun.* **1991**, 1691. Yoshida, M.; Tamada, M.; Asano, M.; Omichi, H.; Kubota, H.; Katakai, R.; Spohr, R.; Vetter, J. *Radiation Effects in Solids* **1993**, *126*, 409.

(15) Foss, C. A.; Hornyak, G. L.; Stockert, J. A.; Martin, C. *J. Phys. Chem.* **1994**, *98*, 2963.

(16) van der Zande, B. M. I.; Bohmer, M. R.; Fokkink, L. G. J.; Schönenberger, C., submitted to *J. Phys. Chem.*

(17) Chlebny, I.; Doudin, B.; Ansermet, J.-Ph. Nano-Structured Materials **1993**, *2*, 637.

(18) Lenczowski, S. K. J.; Schönenberger, C.; Gijs, M. A. M.; de Jonge, W. J. M. *J. Magn. Magn. Mater.* **1995**, *148*, 455.

(19) Fischer, B. E.; Spohr, R. *Rev. Mod. Phys.* **1983**, *55*, 907, see Figure 5 therein.

(20) Ferain, E.; Legras, R. *Nucl. Instr. and Meth. in Phys. Res. B* **1994**, *84*, 331.

(21) Spohr, R.; Ambruster, P.; Schaupert, K. *Radiation Effects and Defects in Solids* **1989**, *110*, 27; Bouffard, S.; Cousty, J.; Pennec, Y.; Thibaudau, F. *Radiat. Eff. Defects Solids* **1993**, *126*, 225.

(22) Musil, C. R.; Jeggle, D.; Lehmann, H. W.; Scandella, L.; Gobrecht, J.; Döbeli, M. *J. Vac. Sci. Technol. B* **1995**, *13 (6)*, 2781.

(23) For a brief review, see: Hatzakis, M. IBM *J. Res. Dev.* **1988**, *32*, 441.